



**HAL**  
open science

## Systematic meteorite collection in the Catalina Dense Collection area (Chile): Description and statistics

Carine Sadaka, Jérôme Gattacceca, Matthieu Gounelle, Mathieu Roskosz,  
Anthony Lagain, Romain Tartese, Lydie Bonal, Clara Maurel, Rodrigo  
Martinez, Millarca Valenzuela

### ► To cite this version:

Carine Sadaka, Jérôme Gattacceca, Matthieu Gounelle, Mathieu Roskosz, Anthony Lagain, et al.. Systematic meteorite collection in the Catalina Dense Collection area (Chile): Description and statistics. *Meteoritics and Planetary Science*, 2025, 10.1111/maps.14307 . hal-04918972

**HAL Id: hal-04918972**

**<https://hal.science/hal-04918972v1>**

Submitted on 30 Jan 2025


**HAL** is a multi-disciplinary open access archive for the deposit and dissemination of scientific research documents, whether they are published or not. The documents may come from teaching and research institutions in France or abroad, or from public or private research centers.

L'archive ouverte pluridisciplinaire **HAL**, est destinée au dépôt et à la diffusion de documents scientifiques de niveau recherche, publiés ou non, émanant des établissements d'enseignement et de recherche français ou étrangers, des laboratoires publics ou privés.



Distributed under a Creative Commons Attribution 4.0 International License

## Systematic meteorite collection in the Catalina Dense Collection area (Chile): Description and statistics

Carine SADAKA <sup>1\*</sup>, Jérôme GATTACCECA<sup>1</sup>, Matthieu GOUNELLE<sup>2</sup>, Mathieu ROSKOSZ<sup>2</sup>,  
Anthony LAGAIN<sup>1,3,4</sup>, Romain TARTESE<sup>5</sup>, Lydie BONAL<sup>6</sup>, Clara MAUREL<sup>1</sup>, Rodrigo MARTINEZ<sup>7</sup>,  
and Millarca VALENZUELA<sup>8,9</sup>

<sup>1</sup>Aix-Marseille Université, CNRS, IRD, INRAE, CEREGE, Aix-en-Provence, France

<sup>2</sup>Muséum National d'Histoire Naturelle, Institut de minéralogie, de physique des matériaux et de cosmochimie—UMR7590,  
Paris, France

<sup>3</sup>Aix-Marseille Université, Institut ORIGINES, Marseille, France

<sup>4</sup>Space Science and Technology Centre, School of Earth and Planetary Sciences, Curtin University, Perth,  
Western Australia, Australia

<sup>5</sup>Department of Earth and Environmental Sciences, The University of Manchester, Manchester, UK

<sup>6</sup>Institut de Planétologie et d'Astrophysique, Université Grenoble Alpes, Grenoble, France

<sup>7</sup>Museo del Meteorito, San Pedro de Atacama, Chile

<sup>8</sup>Universidad Católica del Norte, Antofagasta, Chile

<sup>9</sup>Center of Astrophysics and Associated Technologies CATA, Santiago, Chile

### \*Correspondence

Carine Sadaka, Aix-Marseille Université, CNRS, IRD, INRAE, CEREGE, Aix-en-Provence, France.

Email: [sadaka@cerege.fr](mailto:sadaka@cerege.fr)

(Received 15 July 2024; revision accepted 30 December 2024)

---

**Abstract**—We present the outcome of search campaigns conducted in the Catalina Dense Collection area (DCA) located in the central depression of the Atacama Desert, Chile. The “Catalina Systematic Collection” (CSC) was assembled through systematic on-foot searches, resulting in a total of 1599 meteorites, before pairing, collected over a surface of 6.80 km<sup>2</sup>. This yielded a recovery density of 235 meteorites per km<sup>2</sup> (67 meteorites >20 g per km<sup>2</sup>), making it the densest among hot deserts, even higher than the neighboring El Médano DCA collection. This confirms that the central depression of the Atacama Desert holds the highest meteorite density among hot deserts. We classified 457 meteorites weighing more than 20 g. After correcting for various recovery biases, we estimated a true meteorite density on the ground of 131 meteorites per km<sup>2</sup> for meteorites >20 g before pairing. Using a probabilistic approach, we calculated an average pairing likelihood, yielding 71 meteorites >20 g per km<sup>2</sup> after pairing. This high density is likely linked to an old age of the CSC, which would also explain the absence of carbonaceous chondrites, as they are more prone to alteration by abrasion. This long meteorite accumulation period is related to the long-term hyper-aridity and surface stability of the Atacama Desert, which have persisted for several million years. Meteorites from the CSC show less chemical weathering on average than in other hot deserts, despite the long accumulation period. The H/L ratio in the CSC is higher than in meteorites from other hot deserts, Antarctica, and falls, but similar to the El Médano collection, potentially reflecting variations in the composition of the meteorite flux over the past Myr.

---

## INTRODUCTION

Deserts are the most productive places on Earth for meteorite recovery. This is mainly due to the dry conditions and low erosion, which allow the accumulation and preservation of meteorites over long time scales. During the past decades, tens of thousands of meteorites have been recovered in deserts. While the cold desert of Antarctica accounts for the majority of meteorite finds with around 60% of officially recognized meteorites (Meteoritical Bulletin Database, MBDB, <https://www.lpi.usra.edu/meteor/>, as of December 2024), hot deserts, such as the Arabian Desert (Hofmann et al., 2018; Hofmann & Gnos, 2024), the Sahara Desert (Aboulahtis et al., 2019; Belhai, 2023), deserts in Southwest USA (Zolensky et al., 1990), the Atacama Desert (Gattacceca et al., 2011; Pinto et al., 2024), and the Nullarbor Desert (Benedix et al., 1999; Devillepoix et al., 2022), account for around 35% of classified meteorites. Contrary to the Antarctic case where meteorites are concentrated by glacial processes (Zekollari et al., 2019), the high meteorite densities in hot deserts result from the passive accumulation of meteorites with time. Therefore, besides being an invaluable source of meteorites, hot desert meteorite collections allow assessing the stability of the collection surface, estimating the meteorite flux to the Earth and its possible variations over different time scales (Drouard et al., 2019; Zolensky et al., 1990, 2006), and investigating the rate and effects of terrestrial weathering on meteorites (Al-Kathiri et al., 2005; Pourkhorsandi et al., 2019; Zurfluh et al., 2016).

The Atacama Desert, located in Northern Chile, stands out among hot deserts due to its exceptionally arid and stable climatic conditions. Previous studies indicated that the Atacama Desert is home to the densest hot desert meteorite collections in the world, with up to more than 100 meteorites per km<sup>2</sup> (Gattacceca et al., 2011; Hutzler et al., 2016). In contrast, meteorite densities in other hot deserts are much lower, with about 0.1–1 meteorite per km<sup>2</sup> in the Sahara and 0.57–7.3 meteorites per km<sup>2</sup> in the Arabian Desert (Hofmann et al., 2018; Hofmann & Gnos, 2024). As of today, more than 3700 meteorites from Chile have been listed in the MBDB, most of which have been recovered from DCAs located in the Atacama Desert (Pinto et al., 2024). Furthermore, the Atacama Desert is also a valuable site for collecting micrometeorites, adding another layer of scientific interest to this area (Van Ginneken et al., 2024).

In this study, we focus on the Catalina DCA located in the central depression of the Atacama Desert, extending from 25°18'S to 24°54'S latitude and 70°00'W to 69°30'W longitude. We carried out exhaustive on-foot systematic searches on a single continuous zone during five field campaigns. A total of 1599 meteorites were

recovered over an area of 6.80 km<sup>2</sup>, which is notably higher than any previous systematic study in the Atacama Desert. We call this meteorite collection the Catalina Systematic Collection (CSC). In this work, we present the geological and geomorphological description of the collection area, as well as the statistical properties of the CSC in terms of classification, mass distribution, weathering, pairing, and meteorite density.

## GEOLOGY, GEOMORPHOLOGY, CLIMATE

The Atacama Desert, nestled between the Pacific Ocean and the Andes, is composed of five main geological units: the Coastal Range, the Central Depression, the pre-Andean Range, the Altiplano, and the Western Cordillera. Known as the oldest and driest hot desert in the world (Clarke, 2006), it is characterized by an arid to hyper-arid climate. In the hyper-arid zone, the average annual precipitation does not exceed 5 mm year<sup>-1</sup> (Pfeiffer et al., 2021). The exact age of the onset of the Atacama Desert's aridity remains debated but falls in the 3–25 Ma range (Clarke, 2006; Dunai et al., 2005). This aridity results from a combination of several factors. To the West, the coastal current and the Southeast Pacific anticyclone reduce the advection of Pacific water vapor inland, while to the East, the Central Andes act as a barrier (rain shadow effect), preventing the advection of water vapor from Amazonia to the continental interior (Houston & Hartley, 2003). Due to this long-standing hyper-aridity, some surfaces of the Atacama Desert have not been significantly eroded for millions of years.

In the following, we focus on the central depression where our study area is located. The central depression is an approximately 50 km-wide longitudinal continental basin located West of the Main Cordillera. Its average elevation is around 1000 m in the west and between 2000 and 3000 m in the east. The central depression includes Paleogene–Neogene alluvial, fluvial, and evaporitic sediments, primarily from the Precordillera and Western Cordillera, scattered with thick volcanic ignimbrites (Carretier et al., 2018). The central depression is characterized by low chemical weathering and lacks any fluvial system. It hosts the most productive areas in terms of meteorite recovery, compared to other morphological units (Pinto et al., 2024). The Catalina DCA, in the heart of the central depression, is characterized by a hyper-arid climate with an average annual air temperature range of ~16°C and an average annual cumulative precipitation of ~5 mm year<sup>-1</sup>, recorded between 2001 and 2021 (Pinto et al., 2024).

The CSC area encompasses one main geological formation (Espinoza et al., 2011): the Augusta Victoria Formation (Campanian–Maastrichtian) that includes biotite- and sanidine-bearing rhyolitic pyroclastic rocks.

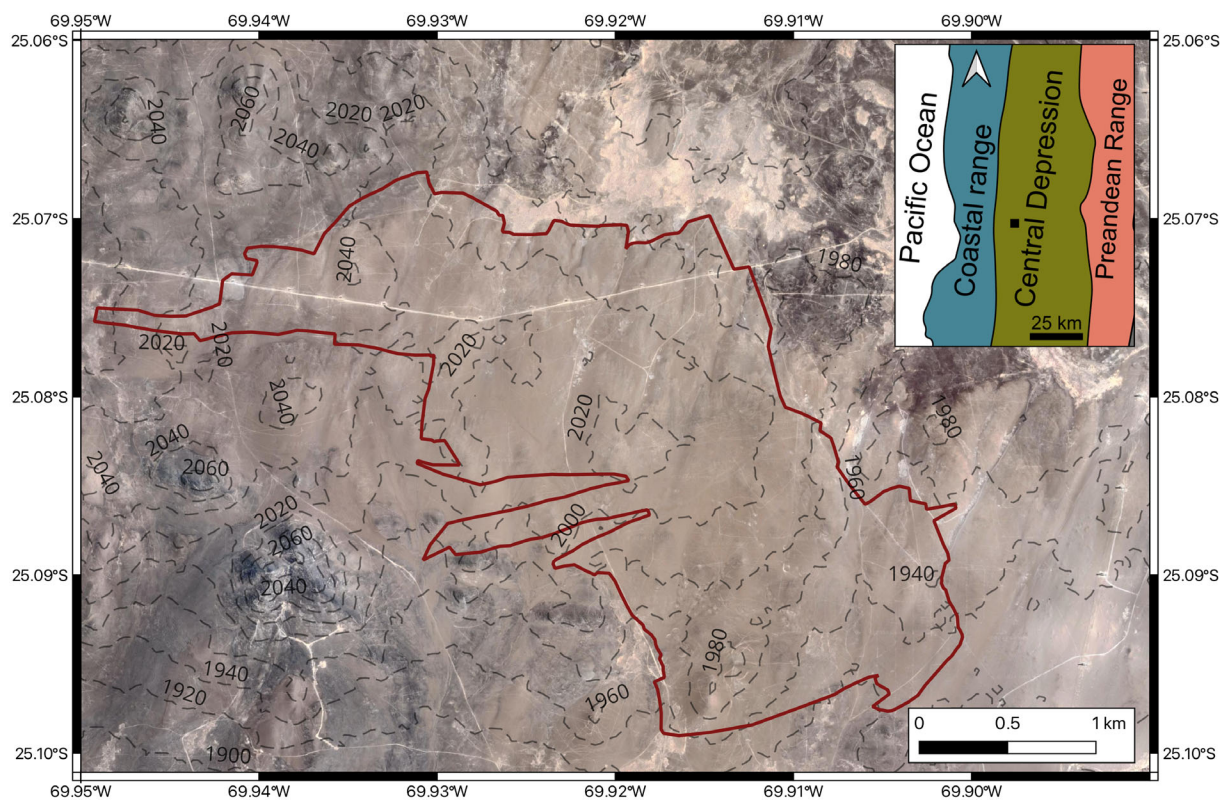


FIGURE 1. Satellite image of the investigated area. The CSC area is outlined in red. Altitude contours are in meters. The insert shows a map of the three main geological units in Northern Chile, with the study area marked by a black square. Google Earth Image.

Outside the searched zone, other formations surround the CSC, of which basaltic and andesitic–basaltic amygdaloidal lavas from the La Negra Formation (middle Jurassic–upper Jurassic), as well as monzodiorites, quartz-bearing monzodiorites, and pyroxene monzonites that are part of the late lower cretaceous Cerro del Pingo plutonic group, and finally, alluvial deposits from upper Miocene–pliocene comprised of poorly stratified gravels with intercalations of coarse sand and silt, some of which contain nitrates (Espinoza et al., 2011).

The CSC area features flat plains with gentle slopes. The surfaces are largely composed of a few centimeters of non-consolidated materials (mostly gravels of igneous rocks) overlying a caliche layer consisting of anhydrite, nitrate, and iodine-rich salts (Tapia et al., 2018). The search area described in this work is a single continuous zone, centered at 25°04'S latitude and 69°55'W longitude, with an altitude range between 1903 and 2054 m above sea level (average altitude of 2046 m), and an average slope of 2° (Figure 1). Despite the presence of numerous volcanic rocks at the surface, the gentle topography and light-colored surface (Figure 2a) make the investigated area very favorable for meteorite recovery.

## METHODS

### Meteorite Recovery

In this study, the collection of meteorites in the Catalina DCA was performed on foot, focusing on a continuous zone on the western side of the DCA. Searches consisted of walking in straight lines at a distance of 8 m from each other, effectively scanning a 4-m area on each side of each searcher. Great care was taken to inspect the surface in a systematic way. For each meteorite found, the GPS coordinates and the distance from the walking line were noted. These samples were collected during five dedicated search campaigns organized by CEREGE (Aix-en-Provence, France) in collaboration with MNHN (Museum national d'Histoire naturelle de Paris, France), the Universidad Catolica del Norte (Antofagasta, Chile), and the Universidad Austral (Valdivia, Chile) in 2017, 2019, 2022, 2023, and 2024. An additional 101 samples were collected by Rodrigo Martínez from Museo del Meteorito (San Pedro de Atacama, Chile). We classified all meteorites with a mass above 20 g, for a total of 457 meteorites. We also



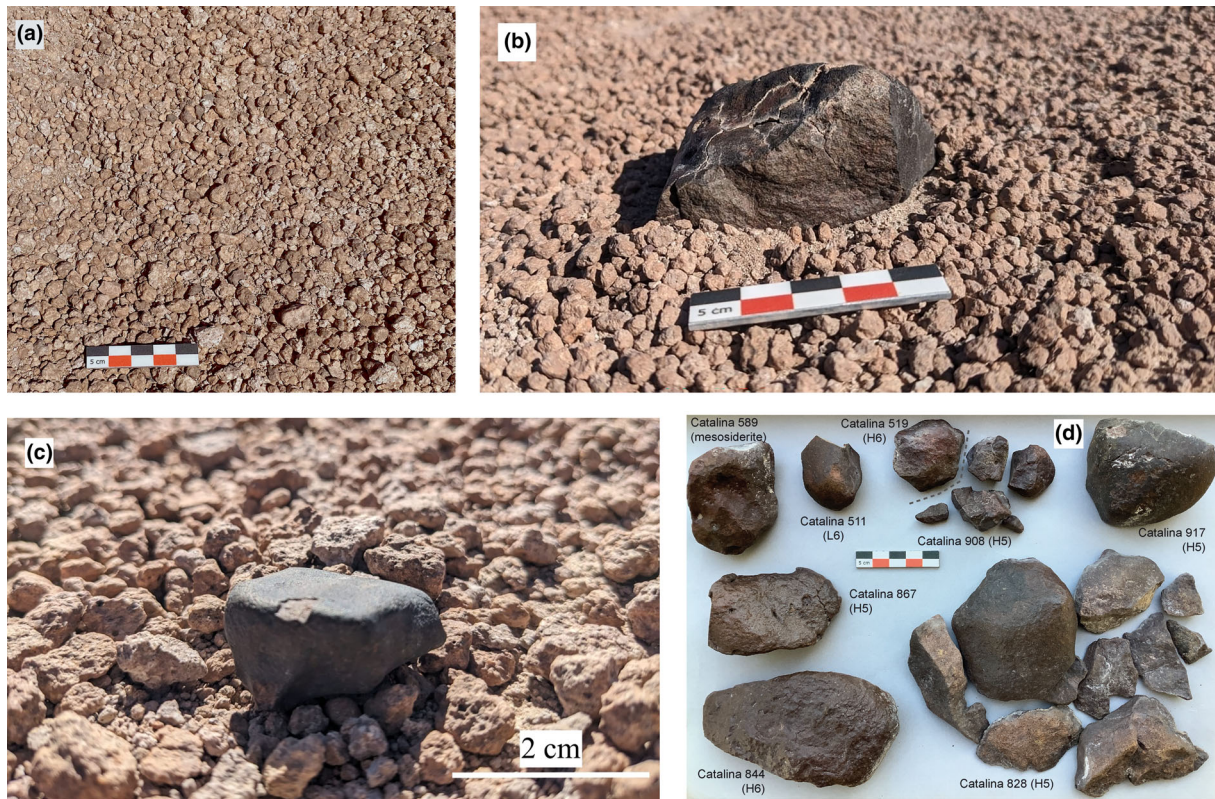


FIGURE 2. (a) Typical surface of the studied zone in the Catalina DCA with a gravel-covered surface. (b) Catalina 827 (LL5, 293 g) in situ. (c) Catalina 905 (L6, 21 g) in situ. (d) Photograph of several Catalina meteorites from the CSC.

classified 65 meteorites weighing less than 20 g, selected based on their unusual aspect or magnetic susceptibility. They include four mesosiderites (Catalina 621, Catalina 629, Catalina 927, Catalina 928), one LL7 (Catalina 462), one L3 (Catalina 570), and one winonaite (Catalina 700). All meteorites classified during this study are listed in the MBDB under the official names Catalina 004, 034, 045–050, 075, 092, 107, 108, 146, 162, 163, 167, 188, 201, 226, 229, 245, 246, 338, 339, 341–343, 399, 409, 410, 423, 424, 426–443, 445–450, 452–460, 462–483, 485–494, 496–498, 500–531, 534–568, 570–573, 575–669, 671–698, 700, 703–731, 734–744, 746–770, 772–793, 797–799, 801–821, 823–934, 948, and 954–958. In the following, except for the mass distribution that takes into account all the recovered 1599 meteorites, only the collection of meteorites  $>20$  g is discussed. Macroscopically, the recovered meteorite samples display a wide range of shapes and preservation states, ranging from rounded or smooth-edged specimens to irregular, shapeless fragments, with some exhibiting a flattened morphology (Figure 2d). Most samples are characterized by a brownish color, and fewer than 10% retained a preserved fusion crust. The meteorites were only slightly buried, and several are covered with a white caliche deposit in their buried part. Many samples consist of several

fragments. For meteorites above 20 g, the average number of fragments is 2.9, usually found over a few  $m^2$ . While chemical weathering is low in the Atacama Desert, meteorites experience fragmentation driven by the formation of iron oxyhydroxides and oxides, and thermoclasty favored by a strong daily temperature cycle inducing high-temperature gradients in the rocks (McKay et al., 2009). Subsequent abrasion by wind and sand processes lead to the gradual disappearance of meteorites. These observations are described in detail in Pinto et al. (2024).

### Classification

Meteorite classification was based on petrography, magnetic properties, and mineral composition. Microscopic petrographic examinations performed with a Leica DM polarizing microscope or a Keyence VHX-7000 digital microscope were conducted on polished sections to examine the mineralogy and texture. Mineral elemental composition was determined by electron probe microanalyses performed at the CAMPARIS facility in Sorbonne Université, Paris, using a Cameca SX Five electron beam ( $\sim 1 \mu m$  in diameter), an accelerating voltage of 15 kV, and a beam current of 10 nA.

The measurement of magnetic susceptibility is a robust, rapid, and nondestructive meteorite classification method, especially for ordinary chondrites (Folco et al., 2006; Rochette et al., 2003). Magnetic susceptibility was measured on whole meteorites at CEREGE using a KLY2 susceptibility meter from Agico equipped with a large coil (65 cm<sup>3</sup>). Samples that did not fit in the coil were measured using an SM30 contact probe from ZH Instruments following the calibration of Gattacceca et al. (2004). The smallest samples (<2 g) were measured with an MFK instrument from Agico or an SM150 instrument from ZH instruments.

## Pairing

Meteoroids often undergo fragmentation during their atmospheric entry, resulting in the fall of multiple stones. Consequently, multiple fragments from the same meteorite are often found scattered within a geographical area called strewn field. Moreover, individual stones may fragment on the Earth's surface due to alteration processes. In dense collection areas, pairing these fragments is challenging and time-consuming regarding data acquisition. However, pairing assessment remains extremely important in any study involving a large meteorite collection, as it can reduce statistical bias and prevent duplicate laboratory analyses (Scott, 1984). Pairing is crucial mostly for equilibrated ordinary chondrites, which are the most abundant types of meteorites.

In our case, of 457 meteorites >20 g, 440 are ordinary chondrites, leading to a staggering 96,580 different possible pairs, making it unrealistic to check each pair of meteorites individually. For these reasons, we tackle the pairing problem using a probability approach with a model similar to that developed by Benoit et al. (2000) and Hutzler et al. (2016). This model can be used for a quick pairing assessment of a large number of meteorites. We modified the model to suit our collection and search area. The mathematical model is coded in Python and available online on GitHub ([https://github.com/csadaka2/ordinary\\_chondrites\\_pairing](https://github.com/csadaka2/ordinary_chondrites_pairing)).

Among the main criteria used in the literature for ordinary chondrites pairing (Benoit et al., 2000; Schlüter et al., 2002), our pairing code incorporates the petrographic type (Van Schmus & Wood, 1967), the weathering grade (Wlotzka, 1993), the fayalite content of olivine, the ferrosilite content of low-Ca pyroxene, the magnetic susceptibility, and the distance between stones. We consider that two meteorites from different groups cannot be paired, so we separated H, L, and LL chondrites. We also assume that unequilibrated ordinary chondrites of type 3 cannot be paired with equilibrated chondrites.

The pairing code was used only for ordinary chondrites, since in our collection, other groups are rare

enough for their pairing to be assessed by checking all possible pairs based on the above-mentioned criteria and petrographic observations. The number of type 3 ordinary chondrites is low enough that whenever pairing was suggested by the pairing code, we checked the possible pairs individually using additional criteria: percentage mean deviation of the fayalite content of olivine, average chondrule size, and other petrographic features (presence of shock veins, melt pockets, polycrystalline troilite, texture of inter-chondrule matrix).

The pairing code calculates a factor  $P$  that reflects the likelihood of two meteorites being paired, using the following equation:

$$P = (\prod_i p_i^{w_i})^{1/\sum w_i}$$

Here,  $p_i$  is the probability of pairing for two meteorites for the given criterion  $i$ , and  $w_i$  is the weight assigned for each criterion  $i$ . Given that some criteria are more robust than others, a different weight was assigned to each (Table 1). Magnetic susceptibility, petrographic type, fayalite content of olivine, and ferrosilite content of low-Ca pyroxene were given a weight of 2, while distance and weathering grade were given a weight of 1. Missing criteria were assigned a weight of zero for mathematical homogeneity.  $P$  is not a probability *stricto sensu*; hence, we use the term factor for mathematical correctness. To invalidate the pairing between two meteorites, it only takes one single criterion being invalid. For this, the weighted geometric mean, where each value is raised to the power of its assigned weight, is a suitable approach for combining probabilities from different criteria when each criterion has a different level of importance. If any of the criteria suggests a very low probability (close to zero), it will significantly impact the overall pairing factor  $P$ , potentially invalidating the pairing. Additionally, each criterion was assigned a probability function. For the weathering grade, petrographic type, and inter-meteorite distance, we applied a discrete function. Magnetic susceptibility, fayalite content, and ferrosilite content probability functions follow a Gaussian distribution, with their standard deviations as listed in Table 1. Therefore, for these properties, the factor  $p_i$  can be computed as the probability that two measurements of a given property for two meteorites ( $x_A$  and  $x_B$ ) are from the Gaussian distribution with a standard deviation  $\sigma$  and a mean value of  $(x_A + x_B)/2$ :

$$p = e^{-\left(\frac{x_A - x_B}{2\sigma}\right)^2}$$

Ordinary chondrite groups have specific ranges of magnetic susceptibility (Rochette et al., 2003, 2012). We chose the parameter  $\sigma$  of the magnetic susceptibility in the pairing code based on the intra-meteorite standard



TABLE 1. Characteristics of the parameters used in the pairing model for the Catalina systematic collection.

Criterion	Distribution	Parameters	Weight
Magnetic susceptibility	Gaussian	0.10	2
Fayalite content	Gaussian	0.63	2
Ferrosilite content	Gaussian	0.61	2
Weathering grade	Discrete	$p = 1$ if $\Delta = 0$ $p = 0.75$ if $\Delta = 1$ $p = 0.5$ if $\Delta = 2$ $p = 0.1$ if $\Delta > 2$	1
Petrographic type	Discrete	$p = 1$ if $\Delta = 0$ or $0.5$ $p = 0.75$ if $\Delta = 1$ $p = 0$ if $\Delta > 1$	2
Distance (m)	Discrete	$p = 1$ if $d < 200$ $p = 0.9$ if $200 < d < 300$ $p = 0.8$ if $300 < d < 400$ $p = 0.7$ if $400 < d < 500$ $p = 0.6$ if $500 < d < 700$ $p = 0.5$ if $700 < d < 900$ $p = 0.4$ if $900 < d < 1000$ $p = 0.3$ if $1000 < d < 1500$ $p = 0.2$ if $1500 < d < 2000$ $p = 0.1$ if $2000 < d < 3000$ $p = 0.05$ if $d > 3000$	1

deviation of magnetic susceptibility measured in OC falls and finds (Table S1). We use a conservative SD of 0.10 for all ordinary chondrite groups.

To have an estimate of the standard deviations for the fayalite content of olivine and the ferrosilite content of low-Ca pyroxene within a given equilibrated ordinary chondrite, we used data from several paired meteorites from strewn fields: the Los Vientos 014 L6 strewn field from the Atacama Desert, the Kumtag L5 strewn field from China (Zeng et al., 2018), and the Jiddat al Harasis 073 L6 strewn field (Gnos et al., 2009). We calculated mean values of the intra-strewn field standard deviation of 0.63 for the fayalite content of olivine and 0.61 for the ferrosilite content of low-Ca pyroxene (Table S2). We use only data from types 5 and 6 ordinary chondrites that represent over 99% of equilibrated ordinary chondrites in the CSC. Standard deviations for the silicate composition of type 4 ordinary chondrites may be higher, especially for low-Ca pyroxene, but are not relevant for this study.

The pairing code returns a symmetrical matrix displaying the pairing factors. These estimates remain qualitative as pairing can never be confirmed with absolute certainty in very dense collection areas, even by checking individual pairs under a microscope. Additional criteria could be used for a more accurate diagnostic of this pairing code: shock stage, presence or absence of specific petrographic features (polycrystallinity of troilite, presence of shock veins, presence of melt pockets, etc.).

## STATISTICS OF THE CSC

### Spatial Distribution

A total of 1599 meteorites, amounting to a total of 52.5 kg, were recovered over 6.80 km<sup>2</sup>. The spatial distribution of the CSC meteorites is shown in Figure 3. Meteorites are found throughout the searched area with no obvious preferential concentration areas or size sorting. The average distance between a meteorite and its closest neighbor is 27 m (Figure 4) and 61 m when considering only meteorites >20 g. These values reflect the extremely high density of meteorites in this area. A small number of meteorites (39) were found immediately outside of our systematic search area by other meteorite hunters (Figure 3). The resulting apparent meteorite density, calculated for the area in Figure 3 that we did not investigate ourselves, is 2.0 meteorites per km<sup>2</sup>, two orders of magnitude lower than the density in the area that we searched in a systematic way (235 meteorites per km<sup>2</sup>), illustrating the efficiency of our collection method. Moreover, the average mass of these 39 meteorites is 50 g, higher than the average mass of 33 g in the CSC (see below), evidencing the incomplete recovery biased toward larger meteorites.

The distribution of magnetic susceptibility (Figure 3), which roughly reflects the distribution of ordinary chondrite groups (Rochette et al., 2003), shows a concentration of meteorites with low susceptibility

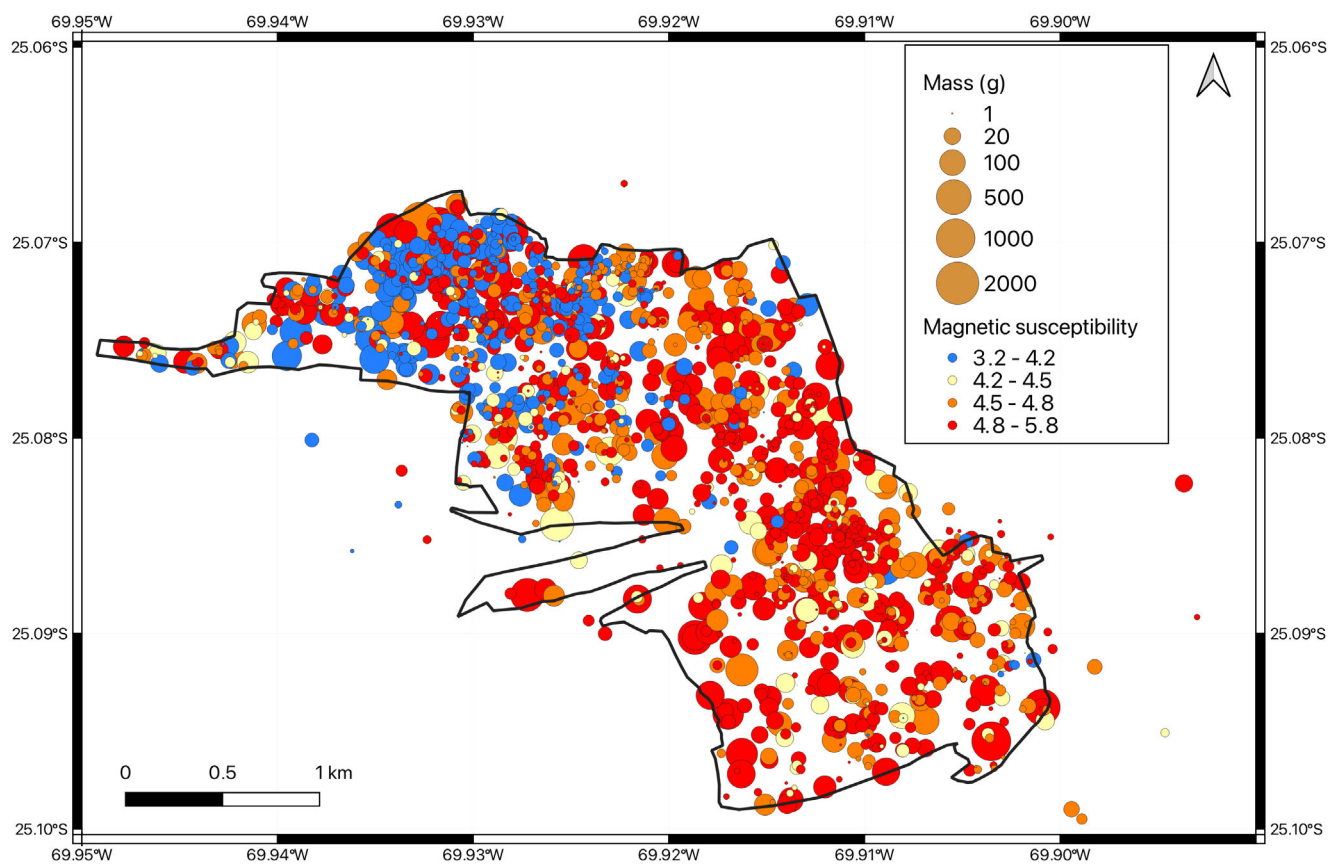


FIGURE 3. Map of the investigated area with the position of the meteorites ( $n = 1599$ ). Meteorites are represented with different sizes reflecting their mass and different colors depending on their magnetic susceptibility values ( $\log\chi$  in  $10^{-9} \text{ m}^3 \text{ kg}^{-1}$ ).

( $\log\chi < 4.2$ ) in the northwestern part of the searched area. This is indicative of a cluster of paired LL chondrites in that area. All 457 meteorites  $> 20$  g have been classified and their spatial distribution is shown in Figure 5.

A concentration of LL5 meteorites is visible in the northwestern part of the area, confirming the existence of an LL5 strewn field in that area. This strewn field contains 262 LL5 samples (including 70 above 20 g), for a total mass of 5.703 kg with no obvious mass-dependent spatial distribution. No significant concentration mechanisms are present that could alter the distribution of meteorites. The gentle slopes ( $2^\circ$  on average) prevent meteorite movements, and the small-scale heterogeneity in slope direction across the study area ensures that any movement would result only in localized and minor redistribution. In this study, we solely focused on meteorites weighing more than 20 g, which are not susceptible to wind-driven movement on flat, gravel-covered surfaces.

### Pairing Detection Using Other Methods

We also evaluated pairing using a cluster analysis algorithm, originally developed for the identification of

crater clusters on planetary surfaces (Automatic Secondary Crater Identification algorithm—ASCI, Lagain et al., 2021), inspired by a protein cluster detection algorithm (Andronov et al., 2016). This tool compares the spatial distribution of the recovered meteorite population in the searched area with a set of randomly distributed meteorite population with a similar number of meteorites over the same area. It then identifies meteorites in clusters with a criteria distance based on their closest neighbors, that is, meteorites are flagged if their presence is unlikely the result of a random stochastic process (meteoritic fall) but rather from a fragmentation process (atmospheric or on the ground). Thus, they are considered paired from a statistical point of view.

This algorithm was applied to the three groups of ordinary chondrites  $> 20$  g described here. Among the 81 LL chondrites, 114 L chondrites, and 245 H chondrites, 48 (59%), 38 (33%), and 59 (24%), respectively, were found to be clustered (Figure 6). The LL chondrite cluster in the NW part of our study area is well identified by the algorithm. Three main other H chondrite clusters and two main L chondrite clusters are also identified and could originate from individual meteorite fall events.



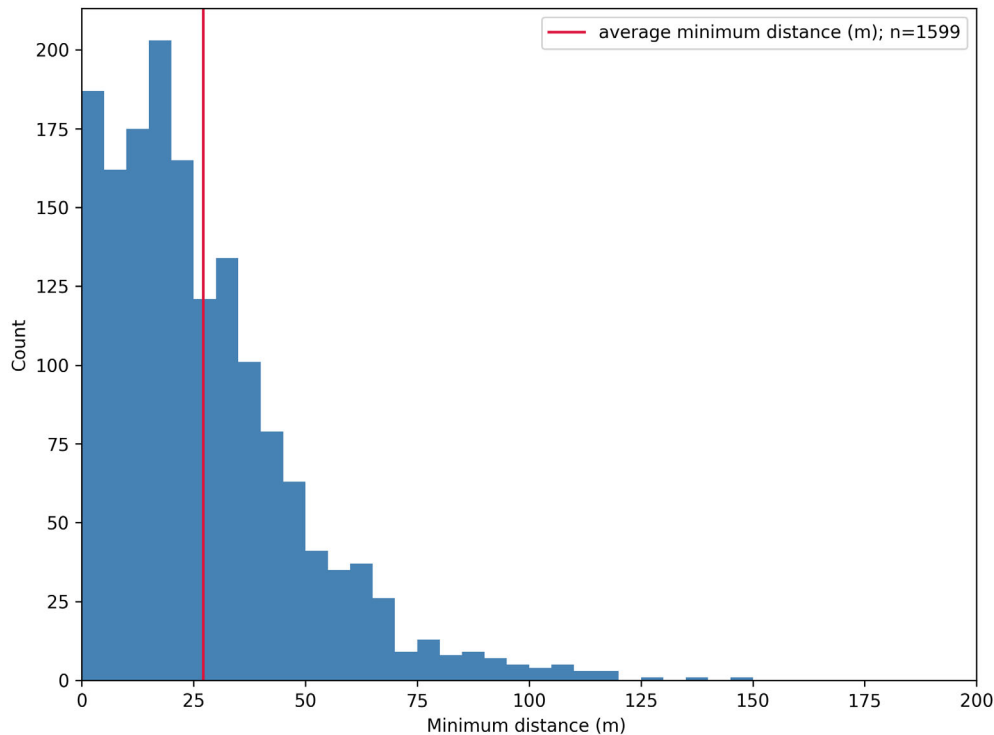


FIGURE 4. Histogram of the distribution of distances to the nearest neighbor of each meteorite ( $n = 1599$ , 10 m bins). The vertical line indicates the mean of 27 m.

Assuming that each cluster represents a single meteorite fall, we obtain 34 LL chondrites, 78 L chondrites, and 189 H chondrites.

Independently, the distance between each meteorite and its closest neighbor was computed within each group (LL, L, and H). A simulation of the same meteorite population randomly distributed across the searched area was conducted and iterated 10,000 times. The average distribution and standard deviation over the 10,000 simulations were computed and compared to the observed distribution (Figure 7). This method highlights the high degree of clustering for LL meteorites: The observed distribution is skewed toward small distances, with 35% of meteorites falling beyond  $1\sigma$  of the simulated random distribution. H and L chondrites also show clustering but to a lesser extent, with 16% and 5% of meteorites beyond  $1\sigma$  of the simulated random distribution, respectively.

### Mass Distribution

Meteorite masses range from 0.31 to 2.183 kg, with 93% weighing less than 100 g and 71% under 20 g, a median mass of 8.9 g, and an average mass of 33 g. The total recovered mass is 52.5 kg. Only one meteorite  $>2$  kg was found, making the CSC depleted in high masses compared to other collections (Table 2). The large

proportion of smaller stones highlights the efficiency of a slow-paced systematic collection that yields smaller specimens compared to searches by car. Moreover, the investigated area has a flat topography and a light-colored surface, enabling the recovery of small meteorites. The cumulative mass distribution of the CSC, shown on a log-number versus log-mass plot, is linear above 135 g with a slope of  $-1.47$  over the 135 g to 1 kg range (Figure 8). Below 135 g, the distribution flattens gradually, likely evidencing the lower efficiency for the recovery of small meteorites. In fact, below a given threshold mass, a flattening can also be observed in the mass distributions of meteorite falls, meteorites from Antarctica and Oman, and from the extensively studied neighboring El Médano systematic collection (Figure 8). It is noteworthy that this threshold mass is variable across the collections: 135 g for CSC and El Médano systematic collection, 1 kg for Oman meteorites, 5 kg for Antarctica meteorites, and 50 kg for meteorite falls. We propose that this threshold mass serves as a proxy for the overall preservation and recovery efficiency of meteorites in a given collection.

### Weathering Grade

The most common weathering grade of meteorites in the CSC is W2 (51%) followed by W1 (37%). We also note the low amount of W3 (10%) and scarcity of W4

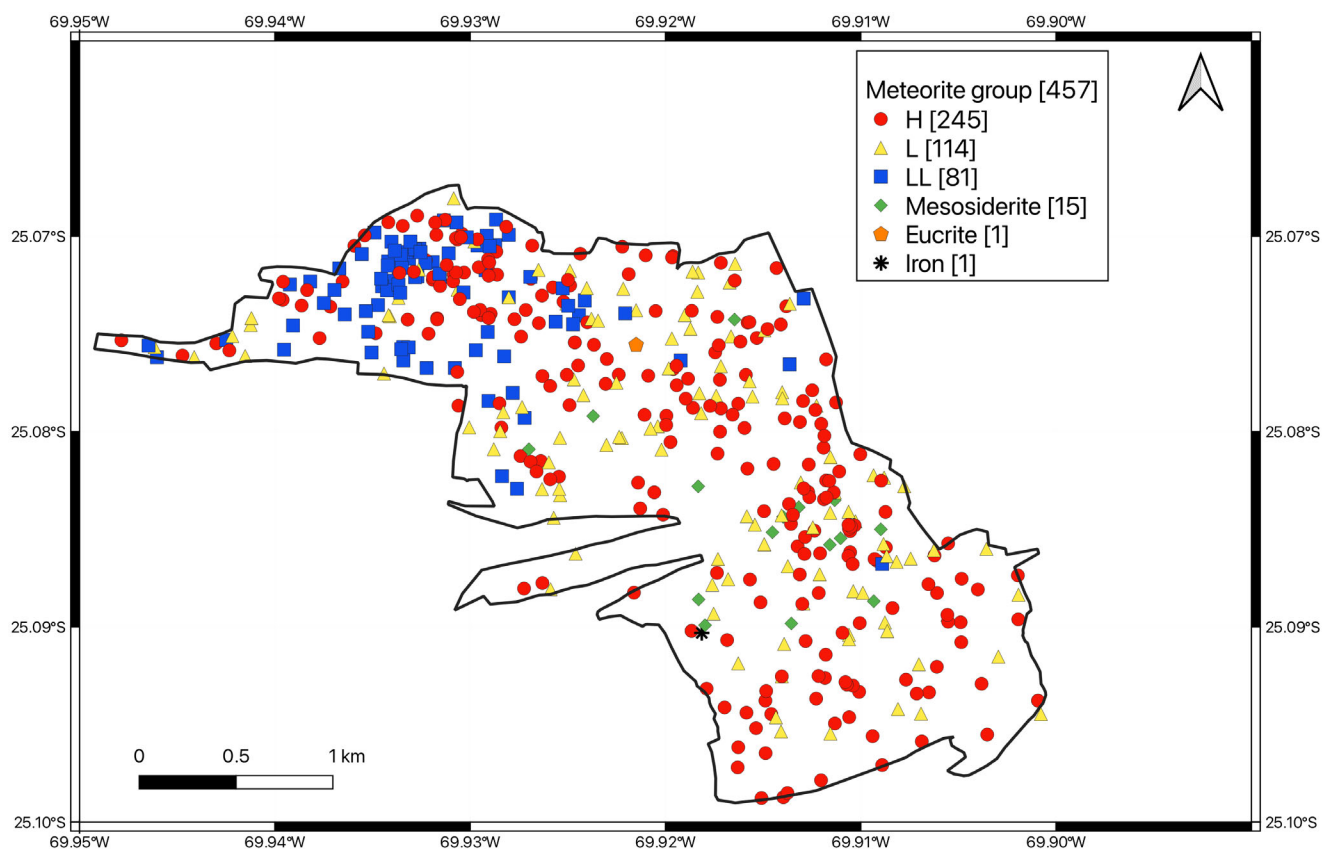


FIGURE 5. Map of the classified meteorites >20 g. The number of meteorites in each group is shown in square brackets.

and above. Since our collection and classification were done systematically, we eliminate the potential bias by hunters or meteorite classifiers for fresh meteorites. We compared the weathering grade distributions in the CSC, the Omani collection, and the Sahara meteorite collection (Figure 9). Despite the non-systematic collection of these samples, their classification was systematic, reducing the bias from the non-declaration of highly altered ordinary chondrites. The meteorites in the CSC are less weathered on average than in other hot deserts. Therefore, this confirms that, despite older surface ages, meteorites from the central depression of the Atacama Desert are better preserved than in hot deserts thanks to the prevailing hyper-aridity (Pinto et al., 2024). The near absence of meteorites with a weathering grade above W3 suggests that rather than chemical processes, physical processes such as fragmentation and abrasion by wind, sand, and dust, are the primary drivers of meteorite removal from the surface of the studied area.

### Group and Type Abundances

The CSC is composed of 96.3% of ordinary chondrites, with 53.6% H, 25.0% L, and 17.7% LL before

pairing (Table 3). Compared to falls, Antarctic meteorites, and other collections in which meteorites have been systematically declared, the CSC is characterized by an overabundance of H and LL chondrites (Table 4). Non-OC meteorites account for 3.7% of the CSC, including 15 mesosiderites, one eucrite, and one iron meteorite (for meteorites >20 g, before pairing). Similar to the other reference collections (modern falls, Antarctic, Oman), the most abundant types in the CSC are H5 and L6 chondrites, with 149 and 92 samples >20 g, respectively, accounting for 60.8% of H chondrites, and 80.7% of L chondrites, before pairing.

Pairing of equilibrated ordinary chondrites was estimated using the pairing model described above. Figure 10 displays the distribution obtained for the pairing factor P among LL, L, and H chondrites of the CSC. We calculated the mean pairing likelihood factor P for each group (Table 3). The number of meteorites after pairing was estimated by simply multiplying the total number of meteorites in a given group by the corresponding mean value of P. The obtained numbers of 22 LL chondrites, 61 L chondrites, and 156 H chondrites are comparable to the results given by the clustering algorithm (34 LL chondrites, 78 L chondrites, and 189 H chondrites).

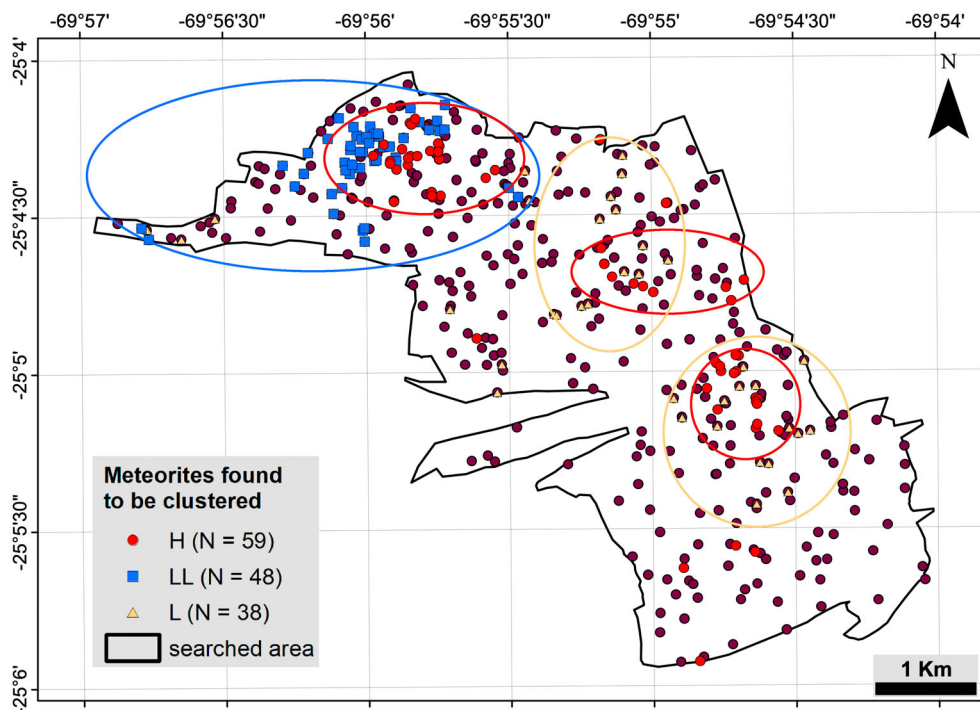


FIGURE 6. Clusters of ordinary chondrites. All meteorites  $>20$  g are shown here, and those recognized as being too close to each other by ASCI are shown in color. Ellipses highlight potential meteorite strewn fields.

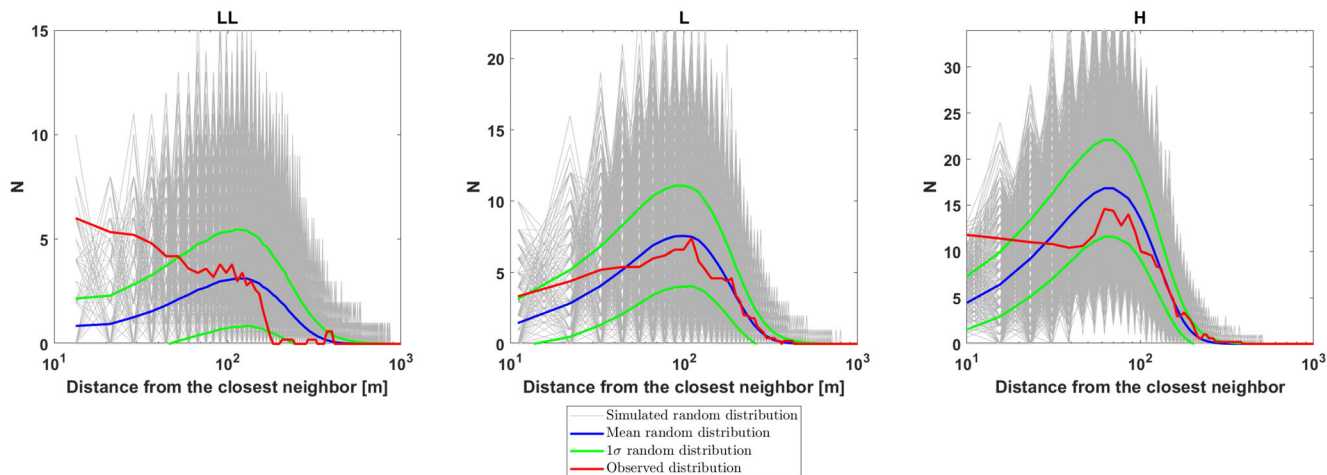


FIGURE 7. Distribution of the observed distance between each meteorite and its closest neighbor within each group (LL, L, and H). Also shown is the simulated random distribution of the same meteorite population across the searched area, iterated 10,000 times. The average distribution and standard deviation over the 10,000 simulations are displayed.

The small number of unequilibrated ordinary chondrites in the CSC (six L3 chondrites and four H3 chondrites) allowed pairing assessment pair by pair, resulting in the tentative pairing of Catalina 815 and Catalina 817 (L3) and Catalina 818 and Catalina 819 (H3). Fifteen mesosiderites  $>20$  g were found in the CSC. Since mesosiderites represent only 0.56% of modern falls (MBDB), pairing is very likely and was assessed pair by

pair using petrographic criteria. Catalina 611 (mesosiderite-A3) differs from other mesosiderites in the CSC by a different texture with exsolution lamellae in pyroxene, different pyroxene composition ( $\text{Fs}_{39}\text{Wo}_3$ ), and higher magnetic susceptibility ( $\log\chi=5.70$ ), suggesting that it represents a different meteorite fall. Catalina 399 (mesosiderites-B2) also differs in texture and composition from the other mesosiderites in the CSC and is not likely



TABLE 2. Ordinary chondrites mass distribution (g) from the CSC, Antarctica, Omani finds, and modern falls.

	CSC OCs	Antarctic OC finds <sup>a</sup>	Omani OC finds <sup>a</sup>	OC falls <sup>a</sup>
Mode	20.0	5.2	62.0	2000
Median	8.75	11.1	185	2580
Mean	31.8	117	1375	22,513
Standard deviation	95.9	2170	12,790	144,331
Minimum	0.31	0.06	0.1	0.1
Maximum	2183	407,000	550,000	4,000,000
Number of meteorites	1577	42,166	4148	966

<sup>a</sup>Data extracted from the Meteoritical Bulletin Database in December 2024.

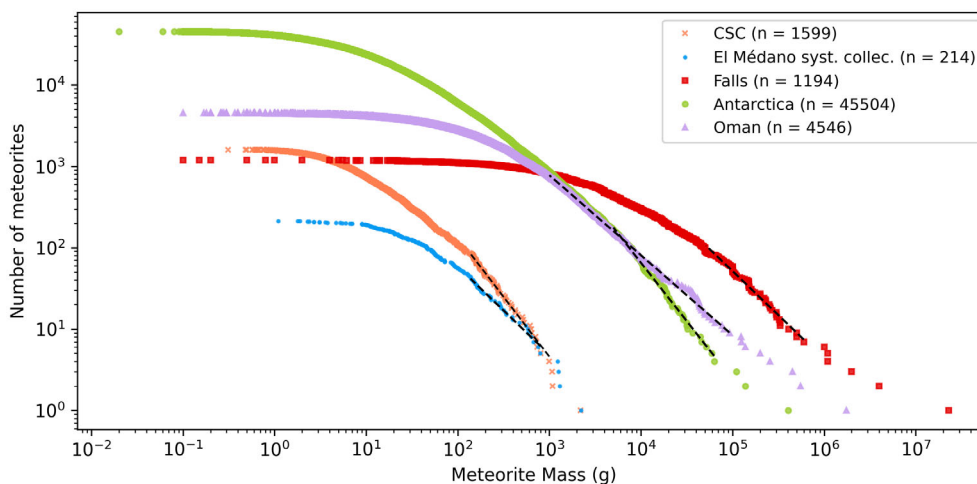


FIGURE 8. Mass distribution of the CSC meteorites (orange crosses,  $n = 1599$ ) on a log–log scale. The linear fit for the mass range from 135 g to 1 kg (dashed line; slope =  $-1.47$ ;  $R^2 = 0.998$ ) is displayed. Also included are the mass distributions of meteorite falls (red squares), as well as meteorites from Antarctica (green spheres) and Oman (purple triangles) (data from MBDB), and meteorites from the El Médano systematic collection (blue dots) (Hutzler et al., 2016). Dashed lines represent the linear fits for each collection over a specific mass range: Antarctica: mass range, 5–100 kg; slope =  $-1.43$ ;  $R^2 = 0.995$ , falls: mass range, 50–900 kg; slope =  $-1.08$ ;  $R^2 = 0.983$ , Oman: mass range, 1–100 kg; slope =  $-0.984$ ;  $R^2 = 0.998$ , and El Médano: mass range, 135 g to 1 kg; slope =  $-1.08$ ;  $R^2 = 0.987$ .

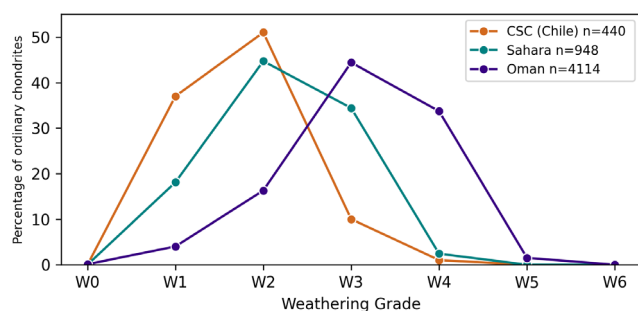


FIGURE 9. Distribution of weathering grade of ordinary chondrites from the CSC (this study), Omani finds, and Sahara finds (Meteoritical Bulletin Database as of December 2024).

paired with them. For the remaining mesosiderites, the following potential pairing groups can be suggested: Catalina 108 and Catalina 581; Catalina 004, Catalina 581,

Catalina 589, Catalina 590, Catalina 591, Catalina 610, Catalina 612, Catalina 820, and Catalina 821. Further measurements such as bulk chemistry, terrestrial age, and cosmic ray exposure age can be of use to confirm the pairing of these mesosiderites. The H/L ratio is 2.15 before pairing and 2.56 after pairing, both of which are significantly higher than the H/L ratio of modern falls (0.88), Antarctic meteorites (1.04), and Omani meteorites (1.35). It is also higher than the H/L ratio of 1.22 for meteorites from other extensively searched Chilean DCAs (Calama, Sierra Gorda, and Chug Chug). It is, however, remarkably similar to the 2.13 H/L ratio of the neighboring El Médano collection (Table 4). Although Kouvatsis and Hofmann (2020) suggested that the H/L ratio is mass dependent and decreases with increasing masses, this observation is not relevant for the CSC. Indeed, in their study, the H/L ratios are constant over the mass range 10 g–1 kg, a range that includes 99% of the meteorites

TABLE 3. Relative abundances by groups and types for meteorites &gt;20 g from the CSC.

Classification	Number	Abundance (%)	Mean $P^a$	Number after pairing	Abundance after pairing (%)
H	245	53.6	0.369	156	63.2
H3	4	1.63		3	1.92
H4	2	0.81		2	1.28
H5	149	60.8		94	60.3
H6	73	29.8		46	29.5
H5-6	15	6.12		9	5.77
H3-5	1	0.41		1	0.64
H3-6	1	0.41		1	0.64
L	114	25.0	0.480	61	24.7
L3	6	5.26		5	8.20
L4	1	0.88		1	1.64
L5	14	12.3		7	11.5
L6	92	80.7		47	77.1
L5-6	1	0.88		1	1.64
LL	81	17.7	0.732	22	8.91
LL3	0	0.00		0	0.00
LL4	0	0.00		0	0.00
LL5	73	90.1		19	86.4
LL6	7	8.64		2	9.1
LL5-6	1	1.23		1	4.6
Mesosiderite	15	3.28		6	2.43
Iron	1	0.22		1	0.40
HED	1	0.22		1	0.40
Total number	457			247	
H/L ratio	2.15			2.56	

Note: For the petrologic type, abundance is within the group.

<sup>a</sup>Mean  $P$  was calculated separately for H, L, and LL chondrites.

TABLE 4. Relative abundances of meteorite groups and types in the CSC before and after pairing, El Médano (Chile), Calama area (Chile), Oman, Antarctica, and falls.

Type	Abundance (%)						
	CSC		El Médano <sup>a</sup>	Calama <sup>b</sup>	Oman <sup>b</sup>	Antarctic <sup>b</sup>	Falls <sup>b</sup>
H	53.6	63.2	62.9	52.4	49.9	40.7	32.1
H5	60.8	60.3	46.3	63.1	39.9	40.8	49.3
H6	29.8	29.5	21.6	16.8	22.9	30.0	24.1
L	25.0	24.7	29.6	42.8	37.1	39.1	36.7
L5	12.3	11.5	6.3	32.0	26.1	39.5	22.5
L6	80.7	77.1	74.6	60.7	56.0	49.4	65.0
LL	17.7	8.91	4.70	2.42	4.53	12.8	8.90
HED	0.22	0.40	0.00	0.31	1.54	1.85	5.59
CC	0.00	0.00	1.90	1.16	1.30	2.98	4.31
Iron	0.22	0.40	0.00	0.18	0.02	0.45	3.91
H/L	2.15	2.56	2.13	1.22	1.35	1.04	0.88
$N$ total	457	247	213	1117	4545	45,509	1252

Note: For the petrologic type, abundance is within the group.

<sup>a</sup>Hutzler et al. (2016).

<sup>b</sup>Data from the MBDB (as of December 2024). Calama meteorites encompass all meteorites from the Calama, Sierra Gorda, and Chug Chug DCA.

classified in the CSC. Moreover, although a detailed discussion is beyond the scope of our study, an updated data set extracted from the MBDB as of December 2024

does not show any dependence of the H/L ratio with mass over the 20 g–10 kg range, neither for falls nor for meteorites from Chile, Libya, and Oman. The

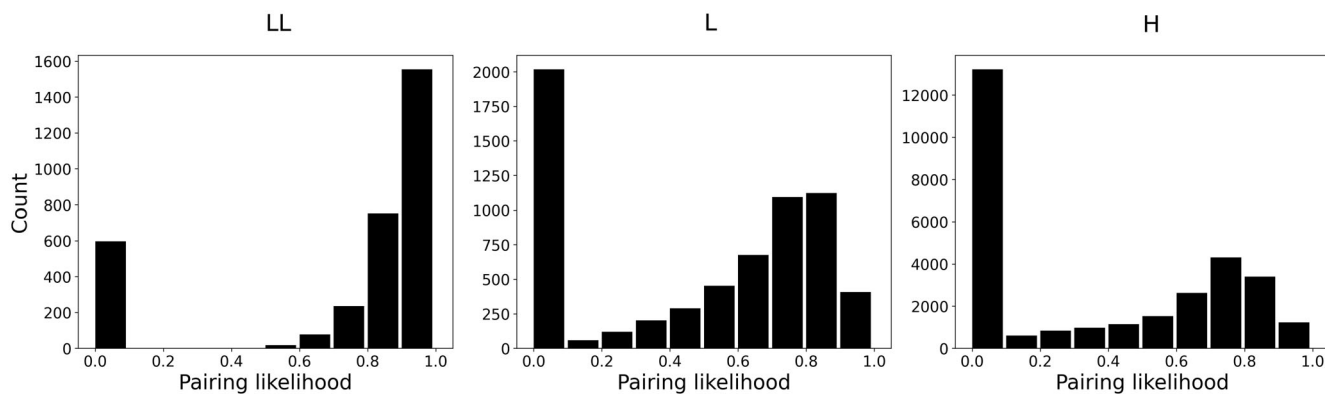


FIGURE 10. Distribution of the pairing likelihood factor  $P$  for LL, L, and H chondrites in the CSC zone for meteorites  $>20$  g, estimated using the pairing code.

overabundance of LL chondrites compared to all other collections (Table 4) is due to the large number of LL5, and persists after pairing, suggesting that our pairing estimate for these meteorites is slightly too conservative. The deficit of HED achondrites in the CSC compared to Oman, Antarctic, and falls collections (Table 4) can be explained by the difficulty in identifying these metal-poor meteorites on the ground when their fusion crust has been abraded because of the presence of numerous terrestrial igneous rocks at the surface. A similar deficit was observed in the El Médano collection (Hutzler et al., 2016). The absence of carbonaceous chondrites in the CSC can be attributed to their fragility and friability, which make them more susceptible to abrasion by wind and sand, the primary driver of meteorite disappearance in the Atacama Desert. This vulnerability reduces their life expectancy at the surface compared to other meteorites, resulting in their lower abundance in old meteorite collections. Finally, the relative scarcity of iron meteorites in the CSC, compared to other world collections could be attributed to their high specific gravity, which causes them to sink and eventually be buried beneath the surface over time (see, e.g., figure 1h in Pinto et al., 2024). Alternatively, it is possible that they were recovered by native peoples in prehistoric and protohistoric times, a practice already documented in other regions of the world (Sparavigna, 2024).

### Meteorite Density

The meteorite recovery density is 235 meteorites per  $\text{km}^2$  (7.73 kg of meteorites per  $\text{km}^2$ ). The recovery density is higher than in any other hot desert, including the neighboring El Médano DCA which yielded 142 meteorites per  $\text{km}^2$  and a mass density of 16.38 kg per  $\text{km}^2$  (Hutzler et al., 2016). The mass distribution of the CSC (Figure 8) shows that the population of meteorites  $<20$  g is biased by incomplete recovery. Therefore, we

only consider the 457 meteorites  $>20$  g in the following discussion. The recovery density of meteorites  $>20$  g is 67 per  $\text{km}^2$ . This is lower than in the El Médano DCA which has 100 meteorites  $>20$  g per  $\text{km}^2$ .

For an accurate estimation of the true meteorite density on the ground, some corrections must be made to account for various recovery biases. The first one involves metal-poor achondrites (mostly HEDs), which are more difficult to spot in the field (see above), iron meteorites, and carbonaceous chondrites. Only one eucrite, one iron meteorite, and no CCs were found among the 457 meteorites  $>20$  g, making up only 0.44% of the CSC, whereas modern falls include 13.82% of HED achondrites, iron meteorites, and carbonaceous chondrites (Table 4). We applied a +13.38% correction factor to take into account this deficit. The second bias involves meteorites missed during systematic research. For each meteorite, we noted the distance between the walking line and the meteorite. Ideally, the meteorites should be found with identical abundances at all distances from the walking lines that are separated by 8 m. However, we note a deficit of meteorites with increasing distance from the line, especially between 2.5 and 4 m from the walking line. In detail, 85% of the meteorites  $>20$  g were found within 2.5 m of the walking line, and only 15% were found in the 2.5–4 m distance interval. If we assume that all meteorites  $>20$  g within 2.5 m of the walking line were recovered, the deficit in the 2.5–4 m interval can be taken into account by applying a +36.0% correction factor to the total number of recovered meteorites  $>20$  g. The third bias is due to the variable efficiency of individual meteorite searchers. A correction was applied for searchers whose number of recovered meteorites was  $2\sigma$  below the average number. Based on yearly recovery statistics, a correction factor of +26% is calculated to take this effect into account. Overall, we estimated that 94.3% of the meteorites  $>20$  g



were not recovered during fieldwork despite careful search. The corrected meteorite density on the ground is 131 meteorites  $>20$  g per km<sup>2</sup>. After pairing, this density goes down to 71 meteorites  $>20$  g per km<sup>2</sup>.

The obtained densities, whatever the mass range and the pairing hypotheses considered, are much higher than in any other hot desert: 0.1 meteorites per km<sup>2</sup> after pairing in Dar al Gani, Libya, 1 meteorite per km<sup>2</sup> in the DCAs of the Sahara (Aboulahris et al., 2019; Schlüter et al., 2002), 2.8 meteorites per km<sup>2</sup> in Saudi Arabia by systematic foot search, 1.1 meteorites per km<sup>2</sup> in Oman through systematic car search, and 7.3 meteorites per km<sup>2</sup> through systematic foot search (Hofmann et al., 2018; Hofmann & Gnos, 2024). However, in specific blowout areas of the Saudi Arabian desert, a density of 150 meteorites per km<sup>2</sup> was found (based on only 21 meteorites found over an area of 0.14 km<sup>2</sup>; Hofmann & Gnos, 2024). The meteorite density in the CSC is matched only by the El Médano area that has estimated densities of 181 meteorites  $>20$  g per km<sup>2</sup> before pairing and of 123 meteorites  $>20$  g per km<sup>2</sup> after pairing, with both densities corrected for the same recovery biases considered for the CSC.

## CONCLUSION

Through systematic on-foot collection, we recovered a total of 1599 meteorites over a continuous zone of 6.80 km<sup>2</sup> in the Catalina DCA. The meteorite recovery density of 235 meteorites per km<sup>2</sup> (67 meteorites per km<sup>2</sup> for stones  $>20$  g) is the highest ever recorded in hot deserts, even surpassing the neighboring El Médano DCA collection. This confirms that the central depression of the Atacama Desert is by far the densest meteorite collection area in hot deserts.

We classified the 457 meteorites above 20 g. After correcting the recovery density for various recovery biases, we estimated a true meteorite density on the ground of 131 meteorites per km<sup>2</sup> for meteorites  $>20$  g before pairing. We used different approaches to assess the pairing of ordinary chondrites; either involving a clustering algorithm, the distance to the nearest neighbor, or a probabilistic approach utilizing a mathematical model. These methods gave comparable results in terms of number of meteorites after pairing. Using the probabilistic approach, we assessed an average pairing likelihood, yielding a meteorite density on the ground of 71 fall events per km<sup>2</sup> after pairing. In the absence of meteorite concentration mechanisms, we interpret this high density as an indication of an old meteorite population, likely several hundreds of kyr by comparison with the El Médano DCA where an  $\sim 700$  ka average terrestrial age has been measured (Drouard et al., 2019). This long meteorite accumulation duration is linked to

the long-term hyper-aridity and associated surface stability over time scales of several Myr. Despite this long accumulation period, meteorites from the CSC are less weathered on average than in other hot deserts. An old age for the CSC meteorites would also explain the absence of carbonaceous chondrites that are more prone to erosion than other meteorites.

The H/L ratio in the CSC is higher than in meteorites from other hot deserts, Antarctica, and falls, but similar to the El Médano collection. This is an indication that the composition of the meteorite flux may have varied over the last Myr. Future work involving measurement of the terrestrial ages of the Catalina meteorite collection will help constrain these possible variations.

*Acknowledgments*—We would like to thank all the people, in addition to the authors, who contributed to the meteorite collection in the CSC area throughout the search campaigns in 2017, 2019, 2022, 2023, and 2024, namely, Jolantha Eschrig, Luigi Folco, Anna Musolino, Chloé Brillatz, Camille Cartier, Marine Ciocco, Foteini Vervelidou, Gabriel Pinto, Kevin Soto, Louna Perez, Anthony Lagain, Lisa Krämer Ruggiu, Katie Joy, Pierre-Marie Zanetta, Lionel Vacher, Audrey Bouvier Nicolas Carcamo, Hamed Pourkhorsandi, Maud Boyet, Pierre Beck, Alexis Drouard, Yves Marrocchi, Maria-Eugenia Varela, Laura Flores, Alexandra Roussopoulos, and Julien Magre. We are grateful to the Meteoritical Society for the Research Grant awarded in 2023 to the first author.

*Data availability statement*—The data that support the findings of this study are available in Meteoritical Bulletin Database at <https://www.lpi.usra.edu/meteor/metbull.php>. Name of meteorites are listed in the manuscript. The pairing code used in this paper is available online on GitHub at [https://github.com/csadaka2/ordinary\\_chondrites\\_pairing](https://github.com/csadaka2/ordinary_chondrites_pairing).

*Editorial Handling*—Richter, Kevin

## REFERENCES

- Aboulahris, M., Chennaoui Aoudjehane, H., Rochette, P., Gattacceca, J., Jull, T., Laridhi Ouazaa, N., Folco, L., and Buhl, S. 2019. Characteristics of the Sahara as a Meteorite Recovery Surface. *Meteoritics & Planetary Science* 54: 2908–28. <https://doi.org/10.1111/maps.13398>.
- Al-Kathiri, A., Hofmann, B. A., Jull, A. J. T., and Gnos, E. 2005. Weathering of Meteorites from Oman: Correlation of Chemical and Mineralogical Weathering Proxies With <sup>14</sup>C Terrestrial Ages and the Influence of Soil Chemistry. *Meteoritics & Planetary Science* 40: 1215–39. <https://doi.org/10.1111/j.1945-5100.2005.tb00185.x>.
- Andronov, L., Orlov, I., Lutz, Y., Jean-Luc Vonesch, J.-L., and Klaholz, B. P. 2016. ClusterViSu, a Method for Clustering of Protein Complexes by Voronoi Tessellation in Super-Resolution Microscopy. *Scientific Reports* 6 (24084): 2045–2322. <https://doi.org/10.1038/srep24084>.

- Belhai, D. 2023. Spatial Distribution and Classification of Algerian Meteorites: Qualitative and Quantitative Inventory. *Journal of African Earth Sciences* 207: 105058. <https://doi.org/10.1016/j.jafrearsci.2023.105058>.
- Benedix, G. K., Keil, K., and Murakami, J. Y. 1999. Classification of Ten New Nullarbor Region Meteorites. *Meteoritics & Planetary Science* 34: 813–15. <https://doi.org/10.1111/j.1945-5100.1999.tb01395.x>.
- Benoit, P. H., Sears, D. W. G., Akridge, J. M. C., Bland, P. A., Berry, F. J., and Pillinger, C. T. 2000. The Non-Trivial Problem of Meteorite Pairing. *Meteoritics & Planetary Science* 35: 393–417. <https://doi.org/10.1111/j.1945-5100.2000.tb01785.x>.
- Carretier, S., Tolorza, V., Regard, V., Aguilar, G., Bermúdez, M. A., Martinod, J., Guyot, J.-L., Hérail, G., and Riquelme, R. A. 2018. Review of Erosion Dynamics along the Major N-S Climatic Gradient in Chile and Perspectives. *Geomorphology* 300(January): 45–68. <https://doi.org/10.1016/j.geomorph.2017.10.016>.
- Clarke, J. D. A. 2006. Antiquity of Aridity in the Chilean Atacama Desert. *Geomorphology* 73: 101–114. <https://doi.org/10.1016/j.geomorph.2005.06.008>.
- Devillepoix, H. A. R., Sansom, E. K., Shoher, P., Anderson, S. L., Towner, M. C., Lagain, A., Cupák, M., et al. 2022. Trajectory, Recovery, and Orbital History of the Madura Cave Meteorite. *Meteoritics & Planetary Science* 57: 1328–38. <https://doi.org/10.1111/maps.13820>.
- Drouard, A. J., Gattacceca, A., Hutzler, P., Rochette, R., Braucher, D., Bourlès, M., Gounelle, M., et al. 2019. The Meteorite Flux of the Past 2 m.y. Recorded in the Atacama Desert. *Geology* 47: 673–76. <https://doi.org/10.1130/g45831.1>.
- Dunai, T. J., González López, G. A., and Juez-Larré, J. 2005. Oligocene–Miocene Age of Aridity in the Atacama Desert Revealed by Exposure Dating of Erosion-Sensitive Landforms. *Geology* 33: 321. <https://doi.org/10.1130/g21184.1>.
- Espinoza, G. F., Matthews, S. J., Cornejo, P. P., and Venegas, B. C. 2011. Carta Catalina-Región de Antofagasta. Serie Geología Básica. Subdirección Nacional De Geología.
- Folco, L., Rochette, P., Gattacceca, J., and Perchiazzi, N. 2006. In Situ Identification, Pairing, and Classification of Meteorites from Antarctica through Magnetic Susceptibility Measurements. *Meteoritics & Planetary Science* 41: 343–353. <https://doi.org/10.1111/j.1945-5100.2006.tb00467.x>.
- Gattacceca, J., Eisenlohr, P., and Rochette, P. 2004. Calibration of Situ Magnetic Susceptibility Measurements. *Geophysical Journal International* 158: 42–49. <https://doi.org/10.1111/j.1365-246x.2004.02297.x>.
- Gattacceca, J., Valenzuela, M., Uehara, M., Jull, T., Giscard, M. D., Rochette, P., Braucher, R., et al. 2011. The Densest Meteorite Collection Area in Hot Deserts: The San Juan Meteorite Field (Atacama Desert, Chile). *Meteoritics & Planetary Science* 46: 1276–87. <https://doi.org/10.1111/j.1945-5100.2011.01229.x>.
- Gnos, E., Lorenzetti, S., Eugster, O., Jull, T., Hofmann, B. A., Al-Kathiri, A., and Eggimann, M. 2009. The Jiddat al Harasis 073 Strewn Field, Sultanate of Oman. *Meteoritics & Planetary Science* 44: 375–387. <https://doi.org/10.1111/j.1945-5100.2009.tb00739.x>.
- Hofmann, B. A., and Gnos, E. 2024. *The Meteoritic Record of Arabia*. Geological Society London Special Publications 550 (1). Geological Society of London: SP550-2024-8. <https://doi.org/10.1144/sp550-2024-8>.
- Hofmann, B. A., Gnos, E., Jull, T., Szidat, S., Majoub, A., Al Wagdani, K., Habibullah, S. N., et al. 2018. Meteorite Reconnaissance in Saudi Arabia. *Meteoritics & Planetary Science* 53: 2372–94. <https://doi.org/10.1111/maps.13132>.
- Houston, J., and Hartley, A. J. 2003. The Central Andean West-Slope Rainshadow and its Potential Contribution to the Origin of Hyper-Aridity in the Atacama Desert. *International Journal of Climatology* 23: 1453–64. <https://doi.org/10.1002/joc.938>.
- Hutzler, A., Gattacceca, J., Rochette, P., Braucher, R., Carro, B., Christensen, E., Cournede, C., et al. 2016. Description of a Very Dense Meteorite Collection Area in Western Atacama: Insight into the Long-Term Composition of the Meteorite Flux to Earth. *Meteoritics & Planetary Science* 51: 468–482. <https://doi.org/10.1111/maps.12607>.
- Kouvatsis, I., and Hofmann, B. A. 2020. A Statistical Analysis of the H/L Ratio of Ordinary Chondrite Finds and Falls: A Comparison of Oman Finds with Other Populations. *Meteoritics & Planetary Science* 55: 67–76. <https://doi.org/10.1111/maps.13410>.
- Lagain, A., Servis, K., Benedix, G., Norman, C., Anderson, S., and Bland, P. A. 2021. Model Age Derivation of Large Martian Impact Craters, Using Automatic Crater Counting Methods. *Earth and Space Science*, 8: ae2020EA001598. <https://doi.org/10.1029/2020ea001598>.
- McKay, C. P., Molaro, J. L., and Marinova, M. M. 2009. High-Frequency Rock Temperature Data from Hyper-Arid Desert Environments in the Atacama and the Antarctic Dry Valleys and Implications for Rock Weathering. *Geomorphology* 110: 182–87. <https://doi.org/10.1016/j.geomorph.2009.04.005>.
- Pfeiffer, M., Morgan, A. M., Heimsath, A. M., Jordan, T. E., Howard, A. D., and Amundson, R. 2021. Century Scale Rainfall in the Absolute Atacama Desert: Landscape Response and Implications for Past and Future Rainfall. *Quaternary Science Reviews* 254: 106797. <https://doi.org/10.1016/j.quascirev.2021>.
- Pinto, G. A., Tavernier, A., Gattacceca, J., Corgne, A., Valenzuela, M., Luais, B., Flores, L., Olivares, F., and Marrocchi, Y. 2024. Dense Collection Areas and Terrestrial Alteration of Meteorites in the Atacama Desert. *Meteoritics & Planetary Science* 59: 351–367. <https://doi.org/10.1111/maps.14125>.
- Pourkhorsandi, H., Gattacceca, J., Rochette, P., D’Orazio, M., Kamali, H., Avillez, R., Letichevsky, S., et al. 2019. Meteorites from the Lut Desert (Iran). *Meteoritics & Planetary Science* 54: 1737–63. <https://doi.org/10.1111/maps.13311>.
- Rochette, P., Gattacceca, J., and Lewandowski, M. 2012. Magnetic Classification of Meteorites and Application to the Sootmany Fall. *Meteoritics & Planetary Science* 2: 67–71. <https://doi.org/10.5277/met120108>.
- Rochette, P., Sagnotti, L., Bourot-Denise, M., Consolmagno, G., Folco, L., Gattacceca, J., Osete, M. L., and Pesonen, L. 2003. Magnetic Classification of Stony Meteorites: 1. Ordinary Chondrites. *Meteoritics & Planetary Science* 38: 251–268. <https://doi.org/10.1111/j.1945-5100.2003.tb00263.x>.
- Schlüter, J., Schultz, L., Thiedig, F., Al-Mahdi, B. O., and Abu Aghreb, A. E. 2002. The Dar al Gani Meteorite Field (Libyan Sahara): Geological Setting, Pairing of Meteorites, and Recovery Density. *Meteoritics & Planetary Science* 37: 1079–93. <https://doi.org/10.1111/j.1945-5100.2002.tb00879.x>.

- Scott, E. R. D. 1984. Pairing of Meteorites Found in Victoria Land, Antarctica. *Memoirs of National Institute of Polar Research* 35: 102–125.
- Sparavigna, A. C. 2024. Meteoric Iron in Ancient Egyptian and Chinese Cultures, from Pyramids to Circumpolar Stars. *SSRN Electronic Journal*. <https://doi.org/10.2139/ssrn.4113311>.
- Tapia, J., González, R., Townley, B., Oliveros, V., Álvarez, F., Aguilar, G., Menzies, A., and Calderón, M. 2018. Geology and Geochemistry of the Atacama Desert. *Antonie Van Leeuwenhoek* 111: 1273–91. <https://doi.org/10.1007/s10482-018-1024-x>.
- Van Ginneken, M., Wozniakiewicz, P. J., Brownlee, D. E., Debaille, V., Corte, V. D., Delauche, L., Duprat, J., et al. 2024. Micrometeorite Collections: A Review and their Current Status. *Philosophical Transactions of the Royal Society a Mathematical Physical and Engineering Sciences* 382: 20230195. <https://doi.org/10.1098/rsta.2023.0195>.
- Van Schmus, W. R., and Wood, J. A. 1967. A Chemical-Petrologic Classification for the Chondritic Meteorites. *Geochimica et Cosmochimica Acta* 31. Elsevier BV: 747–765. [https://doi.org/10.1016/s0016-7037\(67\)80030-9](https://doi.org/10.1016/s0016-7037(67)80030-9).
- Wlotzka, F. 1993. A Weathering Scale for the Ordinary Chondrites (Abstract). *Meteoritics* 28: 460.
- Zekollari, H., Goderis, S., Debaille, V., Van Ginneken, M., Gattacceca, J., Jull, T., Lenaerts, J. T. M., Yamaguchi, A., Huybrechts, P., and Claeys, P. 2019. Unravelling the High-Altitude Nansen Blue Ice Field Meteorite Trap (East Antarctica) and Implications for Regional Palaeo-Conditions. *Geochimica et Cosmochimica Acta* 248: 289–310. <https://doi.org/10.1016/j.gca.2018.12.035>.
- Zeng, X., Li, S., Leya, I., Wang, S., Smith, T., Li, Y., and Wang, P. 2018. The Kumtag 016 L5 Strewn Field, Xinjiang Province, China. *Meteoritics & Planetary Science* 53: 1113–30. <https://doi.org/10.1111/maps.13073>.
- Zolensky, M., Bland, P., Brown, P., and Halliday, I. 2006. Flux of Extraterrestrial Materials. In *Meteorites and the Early Solar System II*, edited by D. S. Lauretta & H. Y. McSween Jr., 853–896. University of Arizona Press.
- Zolensky, M. E., Wells, G. L., and Rendell, H. M. 1990. The Accumulation Rate of Meteorite Falls at the Earth's Surface: The View from Roosevelt County, New Mexico. *Meteoritics* 25: 11–17. <https://doi.org/10.1111/j.1945-5100.1990.tb00965.x>.
- Zurfluh, F. J., Hofmann, B. A., Gnos, E., Eggenberger, U., and Jull, A. J. T. 2016. Weathering of Ordinary Chondrites from Oman: Correlation of Weathering Parameters With <sup>14</sup>C Terrestrial Ages and a Refined Weathering Scale. *Meteoritics & Planetary Science* 51: 1685–1700. <https://doi.org/10.1111/maps.12690>.

## SUPPORTING INFORMATION

Additional supporting information may be found in the online version of this article.

**Table S1.** Intra-meteorite variability of magnetic susceptibility.

**Table S2.** Intra-strewnfield variability of silicate composition in equilibrated ordinary chondrites.